Table 1 Transonic cone boundary layer transition data[a]

M_∞	α deg	α_p deg	$(U/\nu)_\infty \times 10^{-6}$	C_{D_0}	M_δ	$Re_{\delta t} \times 10^{-6}$
1.04	2.5	2.5	0.45 per cm	0.56	0.88	4.4[b] 5.5[c]
1.05	2.8	0.3	0.36 per cm	0.53	0.90	4.7[b] 4.7[c]
1.05	2.7	0.9	0.36 per cm	0.54	0.90	4.5[b] 4.5[c]
1.30	1.4	1.4	0.28 per cm	0.46	1.17	2.9[b] 3.2[c]
1.44	1.7	0.2	0.55 per cm	0.42	1.28	3.9[b] 4.0[c]

[a] For a nominally sharp, smooth cone with semiapex angle = 10. $T_\infty = T_w = 300°$K, and $T_w/T_\delta = 0.95$ in an aeroballistic range.
[b] Only windward-side data, corrected for α effect.
[c] Average of wind and lee data after correction for α effect.

the present data are not claimed to represent ideal or absolute results. They do represent a practical set of conditions free of transonic wind tunnel flow disturbances and thereby provide needed check points for analysis of transonic transition.

The freedom from interference caused by shock reflection from the range wall is explained by noting that the bow shock angle remote from the stagnation point at $M_\infty = 1.05$ is about 15° from a line drawn normal to the centerline. Such a shock would be reflected and return to the centerline more than one body length aft of the cone base in the present case. As an illustration of this, one of the $M_\infty = 1.05$ flights is shown in Fig. 1.

Because small angles of attack existed, the transition Reynolds numbers have been adjusted according to wind-tunnel data on the effect of angle of attack on transition location.[1] The largest adjustment applied to windward data is only −7%, but the largest change of leeward data is +110%. Even though the latter is supported by wind-tunnel data, its magnitude obviously lessens confidence in leeward data.

Table 1 gives the results for the demonstration launches near $M_\infty = 1.05$ plus data for two higher Mach numbers. It would not be prudent to ignore the variation of U/ν or M in efforts to manipulate these data. Many more points would be needed to establish trends of $Re_{\delta t}$ with either $(U/\nu)_\delta$ or M_δ because of the inherent scatter expected in this case.

References

[1] Potter, J. L., "Some Special Features of Boundary-Layer Transition on Aeroballistic Range Models," *Proceedings of Boundary-Layer Transition Specialists Workshop*, Aerospace Corp., San Bernardino, Calif., Vol. III, Sec. 5, Nov. 1971, pp. 1–34.

[2] Potter, J. L., "Observations on the Influence of Ambient Pressure on Boundary-Layer Transition," *AIAA Journal*, Vol. 6, No. 10, Oct. 1968, pp. 1907–1911.

Inverse Transonic Flow Calculations Using Experimental Pressure Distributions

LELAND A. CARLSON*
Texas A & M University, College Station, Texas

Introduction

TRANSONIC airfoil design and analysis is a difficult problem due to the complex interaction between the outer inviscid flow and the viscous boundary layer on the airfoil. Accurate results will require a combination of inviscid and boundary-layer techniques; and any inviscid method utilized must reflect the consequences of any viscous-inviscid interaction.

An attractive inviscid scheme is the inverse method in which the body pressure distribution is prescribed and the corresponding flowfield and effective airfoil shape is determined. This shape can then be used in conjunction with the actual airfoil shape being analyzed to determine the apparent displacement thickness, which can in turn be used as a boundary condition for the viscous analysis. By using displacement thickness instead of pressure, the separation singularity associated with the boundary-layer equations is avoided,[1] and, separated-reversed flow regions can be included in the boundary-layer analysis. Further, since such a viscous solution yields the pressure distribution, the two approaches (inverse inviscid and displacement thickness viscous) may be suitable for an iterative scheme.

Inverse inviscid schemes have previously been presented by Erdos, Baronti, and Elzweig,[2] who used the perturbation potential as the dependent variable, and by Steger and Klineberg,[3] who used velocities. In both cases the methods were actually direct-inverse in that they treated the problem directly (shape given) up to some point and inversely (pressure prescribed) thereafter. Also both schemes could be used to analyze a problem in a completely direct mode. Now it intuitively seems that when direct results obtained with such a scheme are used as input for an inverse calculation, the original body shape should be recovered. Yet, Erdos et al. obtained in that case an apparent discontinuity in body slope at the location of the shock wave, which they attributed to the singular nature of the shock boundary intersection. Steger and Klineberg experienced similar phenomena but determined that they were numerical in origin and that they could be eliminated with careful formulation. Unfortunately, since the two methods used different dependent variables, the self-consistency of an approach using the perturbation potential was not established. This Note shows that self-consistent inverse solutions using the perturbation potential can be obtained and that the results will reflect the effects of viscous-inviscid interaction.

Results

In the present effort a finite-difference relaxation method for solving the nonlinear small perturbation potential equation for transonic flow about airfoils was developed for both direct and mixed direct-inverse calculations. The method utilizes a transformed coordinate system, $\xi = \tanh \alpha_2 x$, $\eta = \tanh \alpha_1 y$, and over relaxation in subsonic zones. Figure 1 shows as the "present method" the airfoil slopes obtained from a direct-inverse

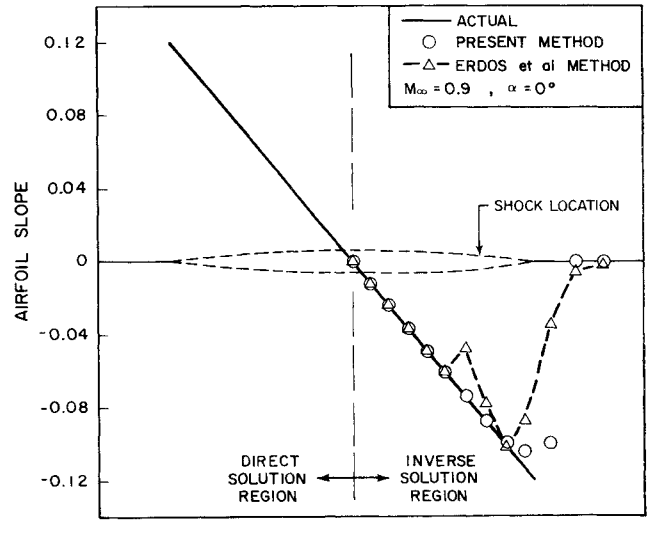

Fig. 1 Comparison of airfoil slopes obtained from inverse method.

Received November 8, 1973. This work was primarily performed while the author was a 1973 NASA-ASEE Summer Faculty Fellow in the Theoretical Aerodynamics Branch at NASA Langley.
Index category: Subsonic and Transonic Flow.
* Assistant Professor, Aerospace Engineering Department.

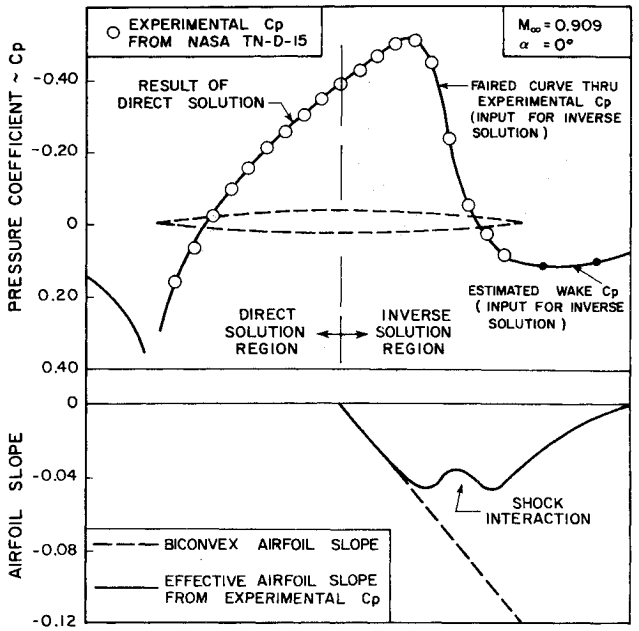

Fig. 2 Results obtained from inverse method using experimental pressures (nonlifting case).

calculation in which the prescribed pressure distribution for the inverse region was obtained from a direct calculation for a 6% biconvex airfoil. In this case the relationship between the pressure and the velocity potential

$$\{\phi_{i,b} = \phi_{i-2,b} - (C_{p_{i-1,b}} \Delta\xi)/[\alpha_2(1-\xi_i^2)]\}$$

was the same in both the direct and inverse regions, and with the exception of the immediate vicinity of the trailing edge the original slope was recovered exactly. (Similar consistent results were also obtained with lifting airfoils.) The method of Erdos et al., however, used in the inverse region the theoretically equivalent expression

$$\{\phi_{i,b} = \phi_{i-1,b} - (C_{p_{i-\frac{1}{2},b}} \Delta\xi)/[2\alpha_2(1-\xi_{i-\frac{1}{2}}^2)]\}$$

but as can be seen on Fig. 1 it yielded a discontinuity in the airfoil slope at the shock wave. Thus, the airfoil slope and shape is sensitive to the method of relating C_p and ϕ, but self-consistent results can be obtained by careful formulation.

To establish that an inverse approach could reflect the consequences of viscous-inviscid interaction, studies were conducted using experimentally determined pressures. Figure 2 shows results for a nonlifting case. The airfoil pressure distribution in the inverse region was obtained from Knechtel,[4] and the wake C_p was estimated. Notice that the C_p distribution computed for the direct region agrees with the measurements and that the variation in airfoil slope indicates significant interaction in the vicinity of the shock wave and the trailing edge. That is, the inverse calculation yielded an effective airfoil shape that exhibits thickening near the shock wave and an open wake, although as will be shown the nature of the latter depends upon the wake C_p distribution. Thus, it appears that the inverse approach can yield results that reflect shock-boundary layer and trailing edge interaction if correct pressures are used.

Results for a lifting case are shown on Fig. 3. Again the airfoil pressures were obtained from Ref. 4 and in the direct-inverse case (solid lines) the wake C_p was estimated. Again, the slope of the effective airfoil exhibits the effects of shock-boundary layer interaction and shows a wake with distinct shape. The latter, indicated by different slopes of the top and bottom "surfaces" in the wake region, is possible since in the inverse case the only boundary condition on the wake is that the pressure (prescribed) be constant across it.

In order to determine the effect of the wake treatment a second case was investigated in which the flowfield aft of the trailing edge was treated directly. This situation, termed direct-inverse-direct, created a downstream Kutta slice across which the change in pressure and vertical velocity must both be zero. Since the effective airfoil trailing edge is not cusped, this approach forces a rear stagnation point to exist. As can be seen on Fig. 3, the direct-inverse-direct results show the same type of shock interaction phenomena as the direct-inverse case. However, downstream of the shock waves the direct-inverse-direct slopes attempt to follow the biconvex airfoil slope in order to satisfy the rear stagnation point criteria. In addition, as required by the boundary conditions, the wake sides are parallel. Obviously, quite different results in the trailing edge region can be obtained depending upon the method of calculating the downstream flow. Of course, the correct result can only be determined by an interactive series of inviscid-viscous calculations in which the wake and possibility of separated flows are included.

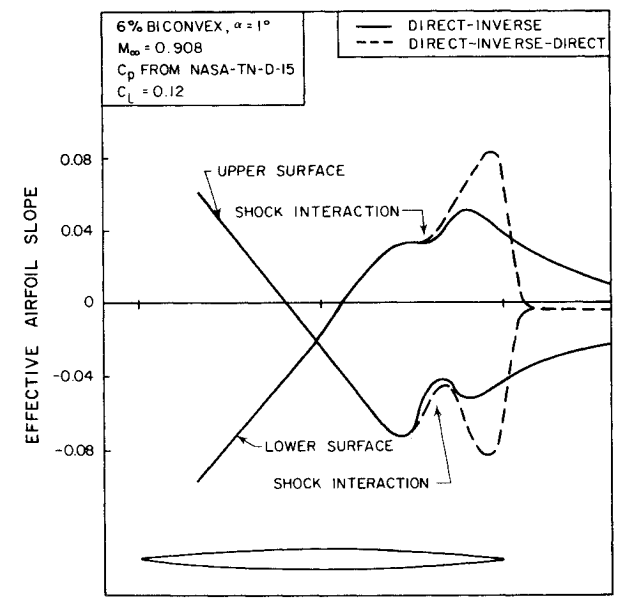

Fig. 3 Airfoil slopes by inverse method using experimental pressures (lifting case).

Conclusions

Based upon these results it is concluded that: 1) inverse transonic flowfield calculations using the perturbation potential as the dependent variable can be obtained which are consistent with direct results; 2) inverse transonic calculations are capable of reflecting the consequences of viscous-inviscid interaction; and 3) near the trailing edge the effective airfoil shape and flowfield structure obtained by the inverse approach depends upon the method of calculating the downstream flow.

References

[1] Catherall, D. and Mangler, K. W., "The Integration of the Two-Dimensional Laminar Boundary-Layer Equations Past the Point of Vanishing Skin Friction," *Journal of Fluid Mechanics*, Vol. 26, Pt. 1, Sept. 1966, pp. 163–182.

[2] Erdos, J., Baronti, P., and Elzweig, S., "Transonic Viscous Flow Around Two-Dimensional Airfoils," AIAA Paper 72-678, Boston, Mass., 1972.

[3] Steger, J. L. and Klineberg, J. M., "A Finite-Difference Method for Transonic Airfoil Design," *AIAA Journal*, Vol. 11, No. 5, May 1973, pp. 628–635.

[4] Knechtel, E. D., "Experimental Investigation at Transonic Speeds of Pressure Distributions Over Wedge and Circular-Arc Airfoil Sections and Evaluation of Perforated-Wall Interference," TN-D-15, Aug. 1959, NASA.